Int J Thermophys (2009) 30:1902–1917
DOI 10.1007/s10765-009-0690-3

Measurement of the In-plane Thermal Diffusivity and Temperature-Dependent Convection Coefficient Using a Transient Fin Model and Infrared Thermography

L. Miettinen · P. Kekäläinen · J. Merikoski · J. Timonen

Received: 15 October 2008 / Accepted: 19 November 2009 / Published online: 1 December 2009

Abstract The transient fin model introduced recently for determination of the in-plane thermal diffusivity of planar samples with the help of infrared thermography was modified so as to be applicable to poor heat conductors. The new model now includes a temperature-dependent heat loss by convective heat transfer, suitable for an experimental setup in which the sample is aligned parallel to a weak, forced air flow stabilizing otherwise the convective heat transfer. The temperature field in the sample was measured with an infrared camera while the sample was heated at one edge. The symmetric temperature field created was averaged over the central fifth of the sample to obtain one-dimensional temperature profiles, both transient and stationary, which were fitted by a numerical solution of the fin model. One of the fitting parameters was the thermal diffusivity, and with a known density and specific heat capacity, the thermal conductivity was thus determined. The test measurements with tantalum samples gave the result $(57.5 \pm 0.2)\,\mathrm{W \cdot m^{-1} \cdot K^{-1}}$ in excellent agreement with the known value. The other fitting parameter was a temperature-dependent heat loss coefficient from which the lower limit for the temperature-dependent convection coefficient was determined. For the stationary state the result was $(1.0 \pm 0.2)\,\mathrm{W \cdot m^{-2} \cdot K^{-1}}$ at the temperature of the flowing air, and its temperature dependence was found to be $(0.22 \pm 0.01)\,\mathrm{W \cdot m^{-2} \cdot K^{-2}}$.

Keywords Convection coefficient · IR camera · Temperature dependence · Thermal conductivity · Thermal diffusivity

L. Miettinen (✉) · P. Kekäläinen · J. Merikoski · J. Timonen
Department of Physics, University of Jyväskylä, P.O. Box 35 (YFL), 40014 Jyväskylä, Finland
e-mail: lasse.m.miettinen@jyu.fi

1 Introduction

The thermal diffusivity of a homogeneous planar sample can be measured with, e.g., the flash method [1], for a recent review, see [2], also in the in-plane direction by using an infrared (IR) camera [3]. There are also other methods that utilize infrared thermography, but the heating of the sample is done differently than in the flash method [4,5]. The convective heat transfer from the sample is taken into account in the latter two methods, and the related heat-transfer coefficient can be determined simultaneously with the thermal-diffusion coefficient.

We referred above to a method that we have previously introduced for determining the in-plane thermal-diffusion coefficient in planar geometry [5]. The method was based on heating a thin planar sample at one end and measuring both the transient and stationary temperature fields in the sample using an IR camera, while introducing at the same time a weak forced flow of air around the sample to stabilize the convective heat transfer from it (see Fig. 1). Since the temperature field was symmetric around the center line of the plate, and the effect of sample edges did not penetrate too far into the sample, we considered the average temperature profile of the central fifth of the plate in the longitudinal direction, and fitted it by the solution of a one-dimensional transient fin model with the thermal diffusion and an effective heat-loss coefficient as the fitting parameters. With a known density and specific heat capacity of the sample, its thermal conductivity could thus be determined. We validated the method by measurements on copper and aluminum samples.

Copper and aluminum are very good conductors of heat, and a natural extension of the method would be to moderately or even poorly conducting materials. To this end, we had to analyze in more detail effects of specific features in the experimental setup. For a relatively poorly conducting sample material, we chose tantalum as its thermal-diffusion coefficient is constant over a wide temperature range around room temperature. It became evident that the two-dimensional temperature field in tantalum samples was not symmetric (see Fig. 2), as in copper and aluminum samples. The reason for this asymmetry was traced to the alignment of the sample perpendicular to the weak flow of air used. The velocity boundary layer that forms on the plate surface grows along the flow direction. The flow velocity is the largest at the lower edge of the plate, and there the convective heat transfer is stronger than at the upper (trailing) edge. For poor heat conductors this obviously leads to an asymmetric temperature field. A simple remedy to this problem was to place the sample parallel to the upward-going air flow with the heated edge up. The heater was placed up because of practical reasons and because then the additional natural convection caused by heating does not interfere too much with the measurement. This setup indeed resulted in a symmetric temperature field, and a one-dimensional temperature profile could again be determined by averaging over a narrow strip around the center line of the sample.

The change in the sample alignment led, however, to a problem with the previously introduced transient fin model. It had been assumed in the model that the heat transfer by convection would be constant in the direction in which the temperature profile was averaged. Now that air was flowing parallel to the gradient of the temperature profile, this assumption was no longer valid: the velocity and thermal boundary layers were

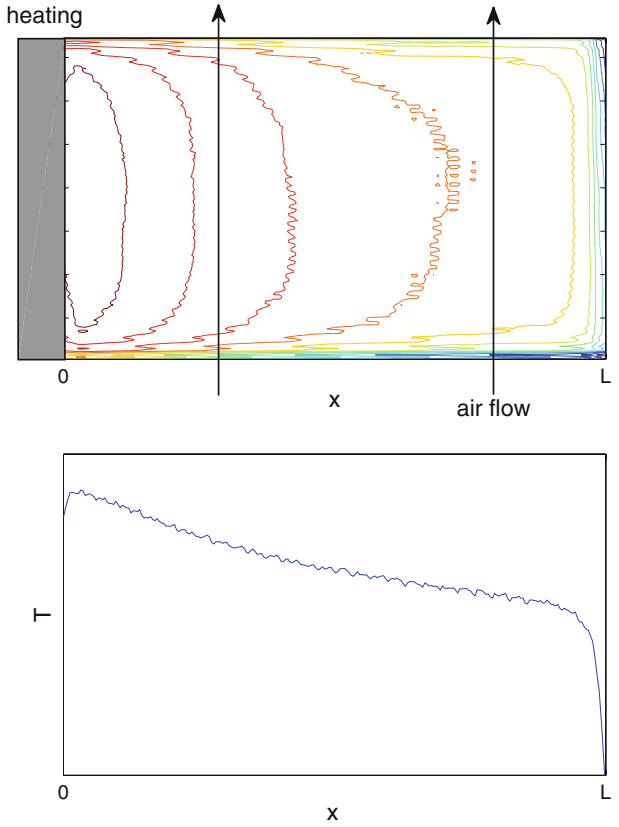

Fig. 1 The principle of our previous experimental method for determining the in-plane thermal diffusivity [5]. The planar sample was heated at one edge while a slow air flow was introduced around the plate. The resulting symmetric temperature field was averaged over the central fifth of the plate in the longitudinal (*horizontal*) direction. The resulting one-dimensional temperature profile (*lower panel*) was then fitted by a fin model

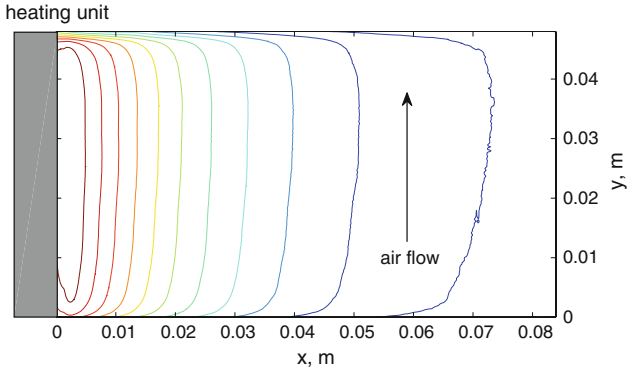

Fig. 2 Isotherms of a stationary temperature field measured on the 0.3 mm thick tantalum sample. The direction of the air flow is indicated. The temperature field does not remain symmetric with respect to the center line in the *x* direction of the sample

increased towards the hot end of the sample, and, consequently, the convective heat-transfer coefficient was also changing. The position dependence of this coefficient had thus to be taken into account, and we modeled the effect by introducing a temperature-dependent coefficient. This meant that the transient fin model became nonlinear, and a new solution to it had to be found.

2 Experimental Method

The experimental setup is described in detail in Ref. [5] apart from the change in the sample alignment. A planar, rectangular (approximately 100 mm × 50 mm) sample initially at room temperature is placed this time vertically in a weak flow of air and heated on the upper end. As before, the purpose of the air flow on both sides of the sample is to stabilize the convective heat transfer. The heating of the upper end of the sample was done by pressing the edge between two hot plates heated by resistors. The temperature evolution of the whole sample was recorded by using an IR camera. For a reliable reading of temperature the emittance of the sample was improved by painting it thinly on both sides with a black spray paint. The IR camera was calibrated for each sample by attaching a thermocouple on the sample surface and measuring the temperature of that point also with the IR camera in the temperature range relevant for the measurements. The possible effect of the paint on the surface temperature of the sample was automatically taken into account by this kind of calibration, and it was not necessary to determine the actual emittance of the sample.

The measured temperature field was averaged as before over the central fifth of the sample so as to obtain a one-dimensional temperature profile along the sample. The time evolution of this profile was then fitted by a solution to the transient fin model with three parameters. The thermal diffusivity is an obvious parameter, and the other two parameters are related to an effective heat-loss coefficient due to convective and radiative heat losses. We previously [5] assumed a constant heat-loss coefficient, but in the present experimental setup we include a linear temperature dependence in this coefficient as described in the following section.

We used two high-purity tantalum plates with known thermal properties (see Table 1) to study the (rather low) thermal diffusivity and the temperature-dependent heat-loss coefficient. The thicknesses of the plates were 0.3 mm and 1.5 mm. They were painted black on both sides. The thicker plate was calibrated so that the temperature measured by the IR camera was corrected to the real surface temperature of the plate as measured by a thermocouple. The calibration curve shown in Fig. 3 was used also for the thinner sample as it was painted with the same paint as the 1.5 mm sample, and the surface finishes of the samples were similar.

Table 1 Thermophysical properties of tantalum at 300 K [7]

Sample	$\rho\left(\mathrm{kg}\cdot\mathrm{m}^{-3}\right)$	$c_p\left(\mathrm{J}\cdot\mathrm{kg}^{-1}\cdot\mathrm{K}^{-1}\right)$	$k\left(\mathrm{W}\cdot\mathrm{m}^{-1}\cdot\mathrm{K}^{-1}\right)$	$\alpha\left(\mathrm{m}^2\cdot\mathrm{s}^{-1}\right)$
Ta	16,600	140	57.5	24.7×10^{-6}

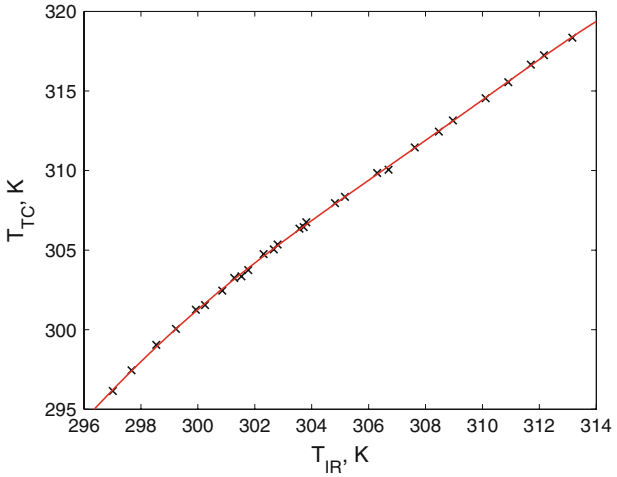

Fig. 3 The temperature calibration curve for the 1.5 mm thick tantalum plate. The apparent temperature was measured by an IR camera and the read surface temperature by a thermocouple

The IR camera images were saved at a rate of 25 frames per second. The one-dimensional temperature profiles were obtained by taking averages over the central fifths of the plates. Furthermore, the stationary measurement data were time averaged over all saved frames in the stationary regime. Next the temperature data were corrected by the calibration curve. Finally the profile data were smoothed by taking a moving average over a small position window (9 pixels, about 3 mm). In the transient measurements the time evolution of the temperature profile was also smoothed by a moving average over 5 frames, i.e., over 0.2 s.

3 Mathematical Model

As before [5], we restrict our consideration to a narrow strip around the center line of the sample plate, and use a one-dimensional transient fin model to describe the system,

$$\rho c_p \frac{\partial T}{\partial t} = \frac{\partial}{\partial x}\left(k\frac{\partial T}{\partial x}\right) - \frac{2h}{a}(T - T_\infty) - \frac{2\varepsilon\sigma}{a}(T^4 - T_\infty^4). \tag{1}$$

Here $T = T(x, t)$ is the (average) temperature profile of the plate with x the distance from its heated edge, and T_∞ is the temperature of the air and the surroundings. The density, ρ, the specific heat capacity, c_p, and the thermal conductivity, k, of the material can to good accuracy be assumed to be constants for tantalum. The thickness of the plate, a, and the emissivity, ε, are also constants. σ is the Stefan–Boltzmann constant, and h is the (position-dependent) convective heat-transfer coefficient, $h = h(x)$.

The temperature of the plate in a stationary situation is thus described by the equation,

$$k\frac{\mathrm{d}^2T}{\mathrm{d}x^2} - \frac{2}{a}h(x)(T - T_\infty) - \frac{2\varepsilon\sigma}{a}(T^4 - T_\infty^4) = 0 \tag{2}$$

with the boundary conditions,

$$\begin{cases} T(0) = T_0 \\ k\frac{\mathrm{d}T}{\mathrm{d}x}(L) + h(L)\,(T(L) - T_\infty) + \varepsilon\sigma\left(T(L)^4 - T_\infty^4\right) = 0, \end{cases} \tag{3}$$

where L is the length of the plate. The convective heat-transfer coefficient h depends on x because of the boundary-layer effects on the air flow across the plate. The functional dependence $h = h(x)$ is *a priori* unknown, and cannot be solved by standard methods applied [7] in the case of a homogeneous temperature in the sample plate (in which case one finds $h(x) \propto x^{-1/2}$; we have also checked that experimental data are not consistent with this kind of position dependence in $h(x)$). We can, however, circumvent this problem as the temperature profile $T = T(x)$ is a monotonic function, and we thus have a one-to-one correspondence between x and T, or rather x and $\Theta := T - T_\infty$. This means that we can also consider x as a function of Θ, $x = x(\Theta)$. We can thus express Eq. 2 in the form,

$$k\frac{\mathrm{d}^2T}{\mathrm{d}x^2} - \frac{2}{a}h(\Theta)(T - T_\infty) - \frac{2\varepsilon\sigma}{a}(T^4 - T_\infty^4) = 0 \tag{4}$$

with an unknown function $h = h(\Theta)$. Since the temperature range in the plate is quite narrow, we can also replace $h(\Theta)$ by its first-order approximation,

$$h(\Theta) = h_0 + h_1\Theta, \tag{5}$$

where h_0 and h_1 are, in principle, functions of T_∞. Variation of T_∞ is, however, so small in the experiments that they can be considered here as constants. This kind of approach has also been used before [6].

Using consistently the notation $\Theta = T - T_\infty$ and substituting the expression Eq. 5 into Eq. 4, expanding the term $T^4 - T_\infty^4$ as a Taylor series with respect to $T - T_\infty$, and retaining only its first two terms, Eq. 4 becomes

$$\alpha\frac{\mathrm{d}^2\Theta}{\mathrm{d}x^2} - \frac{2}{a}\frac{h_0 + 4\varepsilon\sigma T_\infty^3 + \left(h_1 + 6\varepsilon\sigma T_\infty^2\right)\Theta}{\rho c_p}\Theta = 0. \tag{6}$$

Here $\alpha = k/(\rho c_p)$ is the thermal-diffusion coefficient, and we can define

$$\eta := \eta(\Theta) = \eta_0 + \eta_1\Theta = \frac{h_0 + 4\varepsilon\sigma T_\infty^3}{\rho c_p} + \frac{h_1 + 6\varepsilon\sigma T_\infty^2}{\rho c_p}\Theta \tag{7}$$

as an effective temperature-dependent heat-loss coefficient that includes both convective and radiative heat transfer. With this notation, the stationary temperature profile of the plate is determined by

$$\alpha \frac{\mathrm{d}^2\Theta}{\mathrm{d}x^2} - \frac{2}{a}\left(\eta_0 + \eta_1\Theta\right)\Theta = 0. \tag{8}$$

The boundary conditions are now

$$\begin{cases} \Theta(0) = \Theta_0 \\ \alpha \frac{\mathrm{d}\Theta}{\mathrm{d}x}(L) + \left(\eta_0 + \eta_1\Theta(L)\right)\Theta(L) = 0. \end{cases} \tag{9}$$

This boundary-value problem can most easily be solved numerically (an analytical solution exists in terms of elliptic functions, but it is not convenient numerically). We used Matlab and its built-in differential-equation-solver functions to obtain the numerical solution. The two unknown coefficients, η_0/α and η_1/α, can be determined by minimizing the integral,

$$\int_{x_1}^{x_2} \left(\Theta_{(\eta_0/\alpha,\eta_1/\alpha)}(x) - \bar{\Theta}(x)\right)^2 \mathrm{d}x \tag{10}$$

with respect to η_0/α and η_1/α. Here $\Theta_{(\eta_0/\alpha,\eta_1/\alpha)}$ is a solution to the boundary-value problem, Eq. 8 with Eq. 9, and $\bar{\Theta}$ is the measured stationary temperature profile.

The time-dependent case, Eq. 1, can also be written in a similar form,

$$\frac{\partial\Theta}{\partial t} = \alpha \frac{\partial^2\Theta}{\partial x^2} - \frac{2\left(\eta_0 + \eta_1\Theta\right)}{a}\Theta. \tag{11}$$

Notice that Eq. 11 is a nonlinear partial-differential equation. In the experiments one edge of the plate is heated and the time dependence of the edge temperature, $\Theta(0, t)$, is measured. At the opposite edge we have convective and radiative heat transfer. So, in Eq. 11, we impose the initial and boundary conditions,

$$\begin{cases} \Theta(x, 0) = f(x), \\ \Theta(0, t) = \Theta_0(t), \\ \alpha \frac{\partial\Theta}{\partial x}(L, t) + \left(\eta_0 + \eta_1\Theta(L, t)\right)\Theta(L, t) = 0. \end{cases} \tag{12}$$

The initial temperature profile $f(x)$ and the time-dependent edge temperature $\Theta_0(t)$ are known (measured) functions.

Once the parameters η_0/α and η_1/α are extracted from the stationary temperature profile, we can solve numerically the transient case, Eq. 11 with Eq. 12, using Matlab's function called pdepe. Now there is, in principle, only one independent unknown parameter left, the thermal diffusivity, α. But, as carried out previously [5], we search for an optimal solution to the transient problem by letting the η_0/α value obtained from the stationary data vary around the stationary value, and have thereby two fitting

parameters also in the transient case, α and η_0/α. Only the parameter η_1/α is taken as such from the stationary case. Variation of η_1/α would be a higher-order effect.

Our experimental data were thus analyzed in the following way. Two-dimensional optimization with respect to parameters, η_0/α and η_1/α, was performed for the steady-state temperature profile, Eq. 10, as described above. Thereafter, a two-dimensional optimization by minimizing

$$\int_{x_1}^{x_2} \left(\int_{t1}^{t2} \left(\Theta_{(\alpha,\eta_0/\alpha)}(x,t) - \bar{\Theta}(x,t) \right)^2 \mathrm{d}t \right) \mathrm{d}x \tag{13}$$

for the time-dependent temperature profiles $\Theta(x,t)$ was performed with respect to α and η_0/α. The minimum value of Eq. 13 was searched in the vicinity of the η_0/α value obtained for the steady-state profile.

Finally, the convection coefficient h_0 at the reference temperature T_∞ and the temperature dependence h_1 (see Eq. 5) can be solved from Eq. 7:

$$\begin{aligned} h_0 &= k\frac{\eta_0}{\alpha} - 4\varepsilon\sigma T_\infty^3 \\ h_1 &= k\frac{\eta_1}{\alpha} - 6\varepsilon\sigma T_\infty^2. \end{aligned} \tag{14}$$

All the parameters of Eq. 14 are now known from the fitted measurement data ($k = \alpha\rho c_p$) except the emittance ε that we did not determine. However, by using its maximum value of 1.0, we can obtain lower limits for h_0 and h_1.

4 Sensitivity Analysis

It turned out that in transient measurements the temperature rise in the 0.3 mm thick tantalum plate was too small to reliably determine the location of the minimum of the cost function of Eq. 13 in the two-dimensional parameter space. It also became clear that changes in the temperature profile of the 1.5 mm thick sample were too small in the stationary state for optimization by Eq. 10. For these reasons we measured and analyzed only the stationary temperature profile in the 0.3 mm thick sample and the transient temperature profile in the 1.5 mm thick sample.

The same conclusion can also be made based on a sensitivity analysis (see, e.g., [6]) of the heat equation with respect to the fitting parameters. The stationary case, Eq. 8, can be written in the form,

$$\frac{\mathrm{d}^2\Theta}{\mathrm{d}x^2} - \frac{2}{a}\left(\beta_1 + \beta_2\Theta\right)\Theta = 0, \tag{15}$$

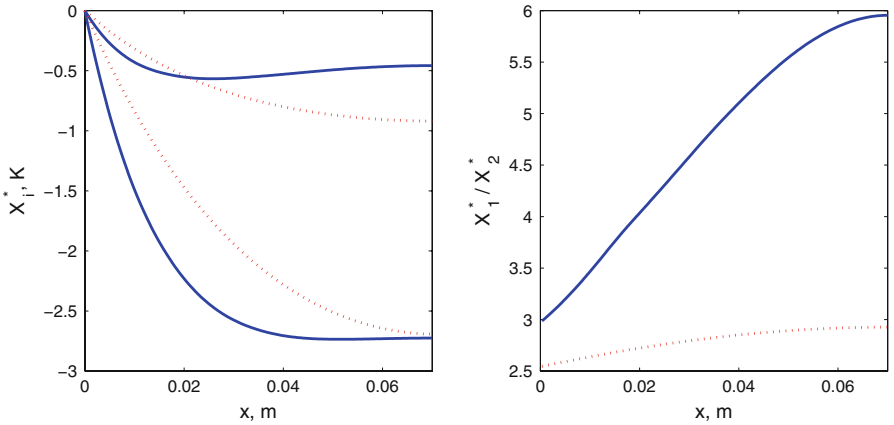

Fig. 4 *Left panel*: reduced sensitivity coefficients X_1^* (*lower curves*) and X_2^* (*upper curves*) for sample thicknesses of 0.3 mm (*solid line*) and 1.5 mm (*dotted line*). *Right panel*: ratio X_1^*/X_2^* for the two sample thicknesses

where we have denoted our two fitting parameters by $\beta_1 = \eta_0/\alpha$ and $\beta_2 = \eta_1/\alpha$. The boundary conditions, Eq. 9, become now

$$\begin{cases} \Theta(0) = \Theta_0 \\ \dfrac{\mathrm{d}\Theta}{\mathrm{d}x}(L) + (\beta_1 + \beta_2\Theta(L))\,\Theta(L) = 0. \end{cases} \tag{16}$$

Reduced sensitivity coefficients can be defined such that [6]

$$X_1^* = \beta_1 \frac{\partial\Theta}{\partial\beta_1} \text{ and } X_2^* = \beta_2 \frac{\partial\Theta}{\partial\beta_2}. \tag{17}$$

These coefficients were determined numerically, and are shown as a function of x in the left panel of Fig. 4. The ratio X_1^*/X_2^* is plotted in the right panel. We used typical measurement values (see Sect. 5): $\Theta_0 = 15\,\mathrm{K}$, $L = 0.07\,\mathrm{m}$, $\beta_1 = 0.13\,\mathrm{m}^{-1}$, and $\beta_2 = 0.0044\,\mathrm{m}^{-1}\cdot\mathrm{K}^{-1}$. Results are shown for two sample thicknesses, $a = 0.3$ mm and $a = 1.5$ mm. It is evident from the ratio X_1^*/X_2^* that parameters β_1 and β_2 are not dependent for the thinner sample. Furthermore, the sensitivity of the method to β_2 is weaker than to β_1, but not too weak to prevent estimation of this coefficient with appropriate precision. For the thicker sample, the ratio X_1^*/X_2^* is nearly constant throughout the sample, and the fitting parameters are thus not independent. Therefore, in the following, if both parameters β_1 and β_2 are determined from stationary data, it is done only for the thinner sample.

5 Results

A stationary temperature field in the 0.3 mm thick tantalum plate is shown in Fig. 5. Isothermal contours show clearly the symmetry of the field, and the window in the

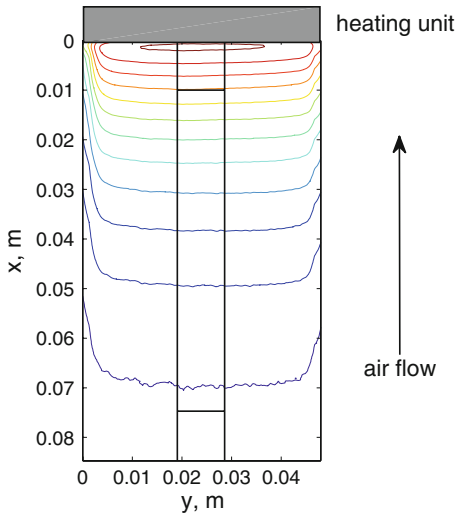

Fig. 5 Isotherms of a stationary temperature field measured on the 0.3 mm thick tantalum sample. The direction of the air flow is indicated. The field was obtained by time averaging over all saved infrared camera frames in the stationary regime. The *vertical lines* border the window in which the mean temperature profile in the x direction was determined. The *short horizontal lines* indicate the interval in the x direction in which the temperature profile of Fig. 6 was fitted by the stationary fin model

vertical direction (x axis), in which the temperature is averaged over the y direction, is marked by straight lines. The resulting mean temperature profile in the x direction is shown in Fig. 6 together with the best theoretical fit based on Eqs. 8–10. The fitted interval in the x direction is indicated by short horizontal lines in Fig. 5, i.e., 10- mm-long intervals at both edges were left out of the fit. The inset in Fig. 6 shows the difference between the data and the fit in more detail. For comparison the corresponding difference is also shown for a linear transient fin model (the one used in Ref. [5]) where the convective heat-transfer coefficient does not depend on temperature. It is evident that the model with the temperature-dependent coefficient provides a better fit. For this particular measurement the parameters that gave the best fit were $\eta_0/\alpha = 0.10693\ \mathrm{m}^{-1}$ and $\eta_1/\alpha = 0.00503\ \mathrm{m}^{-1} \cdot \mathrm{K}^{-1}$, as indicated by the contour lines of the cost function, Eq. 10, shown in Fig. 7.

The fitted results for all the stationary temperature data measured are listed in Table 2. The same results are shown graphically in Fig. 8, where the ratio of the effective heat-loss coefficient (see Eq. 7) to thermal diffusivity is plotted as a function of temperature. Each line corresponds to a result measured in the temperature range given by the end points of the line. The lengths and positions of the lines are thus variable. From Table 2 the averaged final results for the two fitting parameters are $\eta_0/\alpha = (0.121 \pm 0.003)\ \mathrm{m}^{-1}$ and $\eta_1/\alpha = (0.0044 \pm 0.0002)\ \mathrm{m}^{-1} \cdot \mathrm{K}^{-1}$. The error estimates are based on the standard deviation of the mean. The value for the temperature-dependent part of the effective heat-loss coefficient, η_1/α, was used later in the numerical solution of the transient fin model.

Time-dependent temperature profiles from a single measurement in the 1.5 mm thick tantalum plate are shown in Fig. 9 with 12 s intervals. Also plotted in this figure is the best fit by a numerical solution of the transient fin model, Eq. 11, with Eq. 12. As in the stationary case, the last 10 mm of the experimental temperature profile data were left out when optimizing the cost function, Eq. 13. Since the differences between the experimental and numerical data were so small, they are shown separately in Fig. 10.

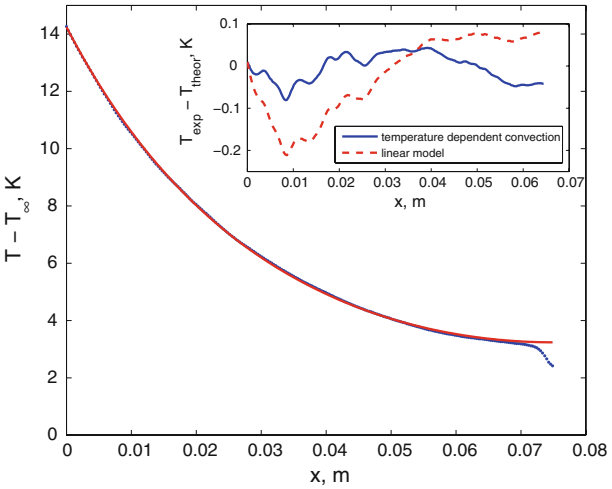

Fig. 6 The stationary temperature profile from the data of Fig. 5 (*dots*) corrected by the calibration curve (Fig. 3) and smoothed by a nine-point moving average. The ambient temperature $T_\infty = 297.8$ K has been subtracted. Note that the first 10 mm interval in the x direction of Fig. 5 is omitted, and the origin has been shifted accordingly. The *solid line* represents the best fit by numerically solving the stationary fin model, Eqs. 8–10. The last 10 mm interval of the measured profile was not used in the optimization. The differences between the data and the fit are shown in the inset for two different fin models. The *dashed line* is the result for our earlier model [5] while the *solid line* is the result for the present fin model with a temperature-dependent convection coefficient

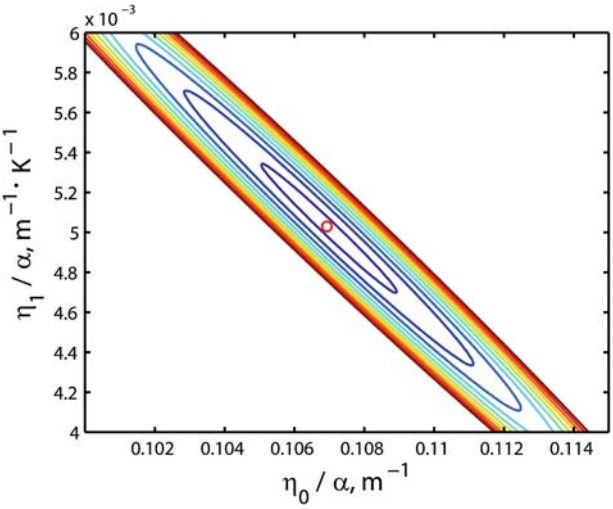

Fig. 7 Contour lines of the cost function, Eq. 10, for the stationary temperature profile of Fig. 6. The best fit is provided by the parameter values, $\eta_0/\alpha = 0.10693\ \mathrm{m}^{-1}$ and $\eta_1/\alpha = 0.00503\ \mathrm{m}^{-1} \cdot \mathrm{K}^{-1}$. The location of the minimum is marked by a *small circle*. The value of the cost function on the innermost contour line is 3 % larger than the minimum value; on the second contour line, it is 13 % larger; and thereafter, *lines* indicate an additional 10 % unit increase in the value

Table 2 Fitted parameter values for the stationary temperature measurements on the 0.3 mm thick tantalum sample, and measured temperature of air flow

Measurement	$\eta_0/\alpha\ \left(\mathrm{m}^{-1}\right)$	$\eta_1/\alpha\ \left(\mathrm{m}^{-1}\cdot\mathrm{K}^{-1}\right)$	T_∞(K)
1	0.11869	0.00501	298.7
2	0.12033	0.00398	298.5
3	0.12262	0.00402	298.4
4	0.11360	0.00462	298.6
5	0.11708	0.00442	298.7
6	0.12083	0.00422	298.6
7	0.13123	0.00417	297.9
8	0.13829	0.00357	298.1
9	0.12366	0.00505	298.2
10	0.10693	0.00503	297.8
Average	0.12133	0.004409	

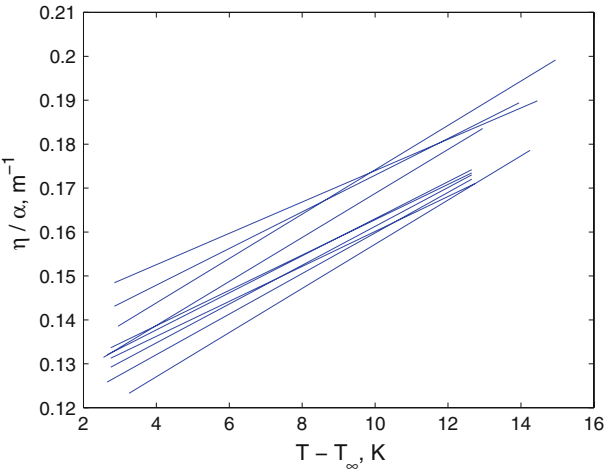

Fig. 8 Results of Table 2 in a graphical form, i.e., $\eta(T-T_\infty)/\alpha = \eta_0/\alpha + \eta_1(T-T_\infty)/\alpha$ as a function of temperature for each individual measurement

They are of the order of 0.1 K at maximum, which is also the accuracy of the IR camera.

The cost function, Eq. 13, together with contour lines are shown in Fig. 11 for the transient temperature data of Fig. 9. In the cost function the parameters were α and η_0/α, but we actually used the thermal conductivity k as a fitting parameter instead of the thermal-diffusion coefficient α, using the known values for the density and specific heat capacity of the tantalum shown also in Table 1. The increments in the parameter values used in the optimization were $0.1\,\mathrm{W}\cdot\mathrm{m}^{-1}\cdot\mathrm{K}^{-1}$ for the thermal conductivity and $0.0001\mathrm{m}^{-1}$ for the parameter η_0/α. The fitted results for all transient-measurement parameters are collected in Table 3. According to our measurements, the thermal conductivity of tantalum is $k = (57.5 \pm 0.2)\,\mathrm{W}\cdot\mathrm{m}^{-1}\cdot\mathrm{K}^{-1}$, which is in excellent

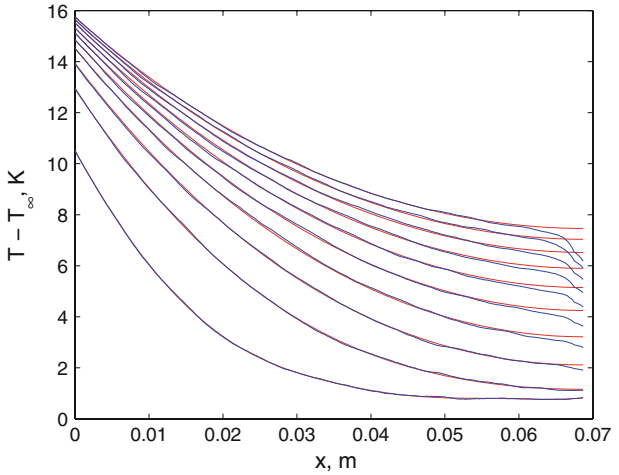

Fig. 9 Transient temperature profiles in the 1.5 mm thick tantalum plate at 12 s intervals together with the best fit by a numerical solution of the transient fin model, Eq. 11, with Eq. 12. The last 10 mm interval of the measured profile was not used in the optimization

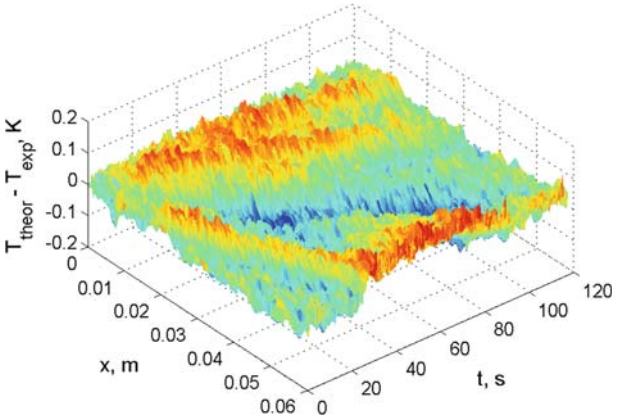

Fig. 10 Difference between the best fit and the measured data of Fig. 9 within the optimization region

agreement with the generally accepted value in the literature, $57.5\,\mathrm{W}\cdot\mathrm{m}^{-1}\cdot\mathrm{K}^{-1}$, while its thermal diffusivity is $\alpha = (24.74 \pm 0.08) \times 10^{-6}\mathrm{m}^2\cdot\mathrm{s}^{-1}$. The parameter $\eta_0/\alpha = (0.158 \pm 0.003)\ \mathrm{m}^{-1}$ was 31 % greater than the value obtained from the stationary measurements, and reasons for this difference are discussed in the next section.

Now that we have estimates for the parameters k, η_0/α, and η_1/α, the lower limits for the components of the temperature-dependent convection coefficient $h(\Theta) = h_0 + h_1\Theta$ can be calculated from Eq. 14 by using the maximal emittance $\varepsilon = 1.0$. For the stationary temperature-field measurements of Table 2, the average values are $h_0 = (1.0 \pm 0.2)\,\mathrm{W}\cdot\mathrm{m}^{-2}\cdot\mathrm{K}^{-1}$ and $h_1 = (0.22 \pm 0.01)\,\mathrm{W}\cdot\mathrm{m}^{-2}\cdot\mathrm{K}^{-2}$. The error limits were taken as the standard deviations of the means. For a typical emittance of 0.8

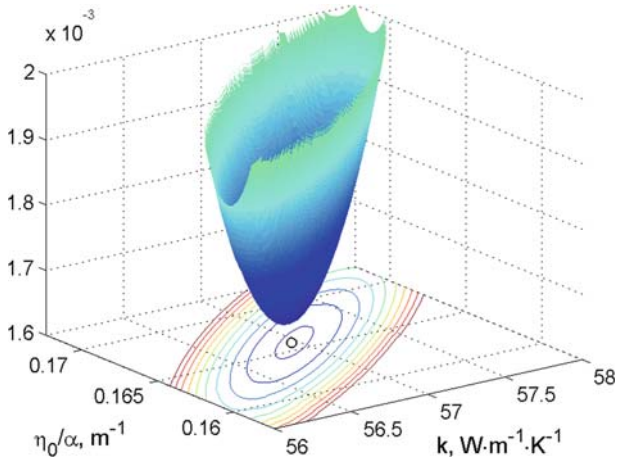

Fig. 11 The cost function, Eq. 13, together with its equal-value contour lines for the transient temperature profiles of Fig. 9. The minimum of the function is indicated by a *small circle*. The value of the cost function on the innermost contour line is 1 % larger than the minimum value, and subsequent contour lines are drawn at 5 % unit increments in the value

Table 3 Fitted parameter values for the transient measurements on the 1.5 mm thick tantalum sample. The values for thermal diffusivity α are related to those of thermal conductivity k by using known values for the density and specific heat capacity of tantalum (Table 1). The measured air flow temperatures are also tabulated

Measurement	$k\left(\mathrm{W\cdot m^{-1}\cdot K^{-1}}\right)$	$\alpha\left(10^{-6}\mathrm{m^2\cdot s^{-1}}\right)$	$\eta_0/\alpha\left(\mathrm{m^{-1}}\right)$	$T_\infty(\mathrm{K})$
1	57.6	24.78	0.1469	298.2
2	57.8	24.87	0.1621	297.8
3	57.0	24.53	0.1565	298.0
4	57.7	24.83	0.1593	298.3
5	57.9	24.91	0.1559	298.2
6	57.0	24.53	0.1658	298.3
Average	57.5	24.74	0.1578	

(gray-body emittance), the convection parameters are $h_0 = (2.2 \pm 0.2)\,\mathrm{W\cdot m^{-2}\cdot K^{-1}}$ and $h_1 = (0.23 \pm 0.01)\,\mathrm{W\cdot m^{-2}\cdot K^{-2}}$. It follows from these values that typically (see Fig. 6) the convective heat-transfer coefficient $h = h_0 + h_1\,(T - T_\infty)$ varied from $3.1\,\mathrm{W\cdot m^{-2}\cdot K^{-1}}$ at the cooler edge of the sample to $5.4\,\mathrm{W\cdot m^{-2}\cdot K^{-1}}$ at the heated edge. Notice that a very low velocity was used in the forced flow induced in the air. For the transient temperature-field measurements (see Table 3), the convection coefficient is at least $h_0 = (3.1 \pm 0.2)\,\mathrm{W\cdot m^{-2}\cdot K^{-1}}$ (emittance of 1.0), while the temperature dependence h_1 is the same as for the stationary case because of the same η_1/α value. For the gray-body emittance $h_0 = (4.3 \pm 0.2)\,\mathrm{W\cdot m^{-2}\cdot K^{-1}}$.

6 Discussion

The thermal conductivity of tantalum was determined surprisingly accurately when the temperature dependence of the effective heat-loss coefficient was incorporated in the stationary and transient fin models. The related addition of one more parameter (h_1) was necessary as evidenced by the minimum value of the cost function, which was reduced by 64 % to 88 % compared to that of the linear fin model when the stationary temperature profiles were analyzed. A similar comparison to the result of the linear model was also made for one transient measurement (measurement number 6 in Table 3). The minimum of the cost function was 30 % higher when the linear model was used, and the fitted thermal conductivity was then $58.3\,\mathrm{W\cdot m^{-1}\cdot K^{-1}}$.

From the stationary temperature measurements on the 0.3 mm thick tantalum sample, we obtained values for the parameters, η_0/α and η_1/α. Although the reference level of the ratio of the effective heat-loss coefficient to the thermal diffusivity, η_0/α, varied slightly between measurements, the slope of its temperature dependence, η_1/α, remained more or less the same as is evident from Fig. 8. That was one of the reasons to use the stationary-state value for η_1/α also when fitting the transient temperature profiles. We tested the sensitivity of the transient fit to this parameter by optimizing the measurement number 6 of Table 3 also with η_1/α values of $0.0042\,\mathrm{m^{-1}\cdot K^{-1}}$ and $0.0046\,\mathrm{m^{-1}\cdot K^{-1}}$, which correspond to the lowest and highest values of this parameter within the error bars. The optimization results for these η_1/α values were $k = 57.025\,\mathrm{W\cdot m^{-1}\cdot K^{-1}}$ and $k = 56.925\,\mathrm{W\cdot m^{-1}\cdot K^{-1}}$, respectively. The increment of the k value was refined to $0.005\,\mathrm{W\cdot m^{-1}\cdot K^{-1}}$ as the difference between the two optimal values was small. By comparing to the k value of $56.95\,\mathrm{W\cdot m^{-1}\cdot K^{-1}}$, which corresponds to an η_1/α value of $0.0044\,\mathrm{m^{-1}\cdot K^{-1}}$, we can say that the uncertainty of the thermal conductivity as determined by our optimization is about $0.1\,\mathrm{W\cdot m^{-1}\cdot K^{-1}}$ with respect to the uncertainty in parameter η_1/α. The deviations between individual measurements are thus larger than the uncertainty of the method. Our result $k = (57.5 \pm 0.2)\,\mathrm{W\cdot m^{-1}\cdot K^{-1}}$ has a smaller uncertainty than the 5 % uncertainty of the accepted thermal conductivity value, $57.5\,\mathrm{W\cdot m^{-1}\cdot K^{-1}}$, for tantalum [7,8].

For the stationary-state data we obtained $\eta_0/\alpha = (0.121 \pm 0.003)\,\mathrm{m^{-1}}$ while $\eta_0/\alpha = (0.158 \pm 0.003)\,\mathrm{m^{-1}}$ for the transient data. This difference can be explained by the different thicknesses of the plates. The transient measurements were done on factor-of-five times thicker sample than for the stationary measurements. Sample thickness can affect the effective heat-loss coefficient η only through the contribution of convective heat transfer. The structure of the flow field of air on both sides of the plate thus seems to depend on sample thickness, causing a thickness dependence also in the convective heat-transfer coefficient. In our previous studies [5] the difference between the optimal η/α values of stationary and transient measurements was only of the order of 1 %, due to the fact that both stationary and transient measurements were carried out on the same sample. As already discussed above, similar effects on η_1/α are much smaller and can be neglected.

Infrared thermography has also been applied to experimental determination of the convective heat-transfer coefficient in a few previous studies, see, e.g., Refs. [9,10]. However, to our knowledge the temperature dependence of the coefficient has not been measured before. With our model, assuming a weak (negligible) temperature depen-

dence of the heat-diffusion coefficient, it is now possible to determine simultaneously both the in-plane thermal diffusivity and the temperature-dependent convection coefficient by measuring the temperature profile in a thin planar sample.

References

1. W.J. Parker, R.J. Jenkins, C.P. Butler, G.L. Abbott, J. Appl. Phys. **32**, 1679 (1961)
2. L. Vozár, W. Hohenauer, High Temp. High Press. **35/36**, 253 (2003/2004)
3. I. Philippi, J.C. Batsale, D. Maillet, A. Degiovanni, Rev. Sci. Instrum. **66**, 182 (1995)
4. B. Rémy, A. Degiovanni, D. Maillet, Int. J. Thermophys. **26**, 493 (2005)
5. L. Miettinen, P. Kekäläinen, J. Merikoski, M. Myllys, J. Timonen, Int. J. Thermophys. **29**, 1422 (2008)
6. J.V. Beck, K.J. Arnold, *Parameter Estimation in Engineering and Science* (Wiley, New York, 1977)
7. F.P. Incropera, D.P. DeWitt, *Fundamentals of Heat and Mass Transfer*, 5th edn. (Wiley, New York, 2002)
8. Y.S. Touloukian, C.Y. Ho, *Thermophysical Properties of Matter, Vol. 1: Thermal Conductivity – Metallic Elements and Alloys* (Plenum Publishing Corp., New York, 1970)
9. G. Maranzana, S. Didierjean, B. Rémy, D. Maillet, Int. J. Heat Mass Transf. **45**, 3413 (2002)
10. A. Grine, D. Saury, J.-Y. Desmons, S. Harmand, Exp. Therm. Fluid Sci. **31**, 701 (2007)